JOURNAL OF MATERIALS SCIENCE 25 (1990) 5303–5312

Deposition characteristics and properties of iron nitride films by CVD using organometallic compound

HIROSHI FUNAKUBO, NOBUO KIEDA, MASANORI KATO, NOBUYASU MIZUTANI
Department of Inorganic Materials, Faculty of Engineering, Tokyo Institute of Technology, 2-12-1 O-okayama, Meguro-ku, Tokyo 152, Japan

TETSUO TATSUNO
Electronic Material Division, Taiyo Yuden Co. Ltd, 1660 Kami Satomi, Haruna-Machi, Gunma 370-33, Japan

Iron nitride films were prepared by chemical vapour deposition from the gas mixture of $Fe(C_5H_5)_2$–NH_3–H_2–CO_2. The effects of deposition parameters on the deposition characteristics were investigated. Iron nitride films were deposited above 500° C and the films of γ'-Fe_4N single phase were deposited above 700° C. At 700° C and under the total gas flow rate from 1 to 8 l min^{-1}, the deposition rate of the film may be controlled by the transport of $Fe(C_5H_5)_2$ molecules to the surface of the deposits. At 700° C and under the total gas flow rate of 4 l min^{-1}, the phases and nitrogen contents of the films were determined by $pNH_3/pH_2^{3/2}$, the controlling factor of the nitrogen contents of the films. Decreasing of the total gas flow rate and increasing pCO_2 increased the nitrogen contents of the films and phases with higher nitrogen were deposited. On the other hand, increasing $pFe(C_5H_5)_2$ and the absence of pCO_2 increases the carbon contents of the films, and the phase with a greater solubility in carbon, i.e. ε-Fe_2N, was codeposited with γ'-Fe_4N. The saturation magnetization of the films deposited at 700° C was in good agreement with that reported for the bulk iron nitride, which depended not on the deposition conditions but on the nitrogen contents of the films.

1. Introduction

In the iron–nitrogen system, γ'-Fe_4N, ε-Fe_2N and ζ-Fe_2N are known to be stable, while α''-Fe_8N exists as a metastable phase at room temperature [1]. Some of iron nitrides, e.g. γ'-Fe_4N and α''-Fe_8N, are promising magnetic recording media because of their excellent magnetic and chemical properties. The saturation magnetization, σ_s, of γ'-Fe_4N is 192 e.m.u. g^{-1} which is as high as 85% of that of iron metal (219 e.m.u. g^{-1}) at room temperature, and σ_s of α''-Fe_8N is estimated to be 298 e.m.u. g^{-1}, which is larger than that of iron metal [2]. Moreover, these nitrides are hard and chemically stable compared with iron metal.

The fine powder preparation of γ'-Fe_4N has been extensively investigated for its practical use as a magnetic recording medium coated with particles. The following preparation methods have been reported: (1) the evaporation of iron metal in nitrogen gas [3, 4]; (2) the gas reaction between $FeCl_2$ and NH_3 [5]; (3) the nitriding of α-Fe or α-FeOOH in an atmosphere of NH_3 or a gas mixture of NH_3 and H_2 [5–8]. However, σ_s of these powders was much lower than the reported value for the bulk γ'-Fe_4N because of the surface oxidation of the powders.

In order to improve this reduction in σ_s, the preparation of iron nitride films has been widely investigated. Various vapour deposition techniques, such as evaporation [2, 9], sputtering [10–14], ion plating [15, 16], ion-beam deposition [17–19] and ion implantation [20–22] have been attempted in order to synthesize the iron nitride films with high σ_s. Some of these techniques were successful in obtaining the films with a higher σ_s than that of α-Fe [2, 10, 17, 18, 21]. This extremely high value was considered to be due to the formation of the α''-Fe_8N. However, the films with high σ_s did not always consist of α''-Fe_8N and the relationship between this high σ_s and the existence of α''-Fe_8N was not revealed. Moreover, the effects of the deposition parameters on the characteristics of the deposits, e.g. the composition of the films, are very complicated in these techniques, and have not been elucidated. This is mainly due to the fact that deposition occurs under conditions which are far from the equilibrium.

Chemical vapour deposition (CVD) is a method for forming films through chemical reactions among gas species under near-equilibrium conditions. Therefore, it is expected that the films are deposited reproducibly and controllably compared with the techniques described above. Saito *et al.* [23] prepared hexagonal

0022–2461/90 $03.00 + .12

ε-Fe_2N films by plasma-assisted CVD using a gaseous mixture of $Fe(CO)_5$–NH_3–H_2 for application as a perpendicular magnetic recording medium. They reported that the films deposited at 200° C were oriented to the *c*-axis and the coercive force parallel to the plane of the films was 2.1 times larger than that of the transverse one. However, only one paper has reported the preparation of the iron nitride films by CVD.

We have already reported the synthesis of iron nitride films by CVD using $Fe(C_5H_5)_2$, NH_3, H_2 and CO_2 as source materials under atmospheric pressure and showed that the composition of the deposits could be controlled by the partial pressure of NH_3 and H_2 at the deposition temperature of 700° C [24]. Here we describe further details of the preparation of iron nitride films. Moreover, the effects of the deposition parameters, such as deposition temperature, total gas flow rate, and the partial pressure of each composition gas on the deposition rate, the phases, microstructures, nitrogen and carbon contents, and magnetic properties of the deposits, were examined.

2. Experimental procedure

The iron nitride films were prepared from a gaseous mixture of $Fe(C_5H_5)_2$–NH_3–H_2–CO_2. Ferrocene, $Fe(C_5H_5)_2$, is a suitable source material for CVD because of its high vapour pressure at relatively low temperature [25, 26]. In addition, the bonds between iron and cyclopentadiene (Fe–Cp) are much weaker than the bonds within the Cp rings, so that Fe–Cp bonds should be primarily broken when the ferrocene vapour was decomposed to deposit films [27]. Therefore, it is expected that the carbon content of the deposits can be reduced. CO_2 was also introduced into the system with the intention of reducing the carbon contents of the deposits according to the equation

$$CO_2 + C \rightarrow 2CO \quad (1)$$

A schematic diagram of the CVD apparatus used in the present study is shown in Fig. 1. The ferrocene vapour was generated by heating the ferrocene powder (Tokyo Kasei Co., Ltd) and carried to the substrate by nitrogen gas. The evaporation rate of ferrocene was controlled by the heating temperature ranging from 180 to 250° C and determined from the weight loss of ferrocene powder during each experimental run. The ferrocene vapour was mixed with NH_3, H_2, CO_2 and N_2 by a static mixer. Nitrogen was used as the balancing gas to keep the total gas flow rate constant for the variation of the gas composition. It has been confirmed previously by substituting nitrogen for argon that the partial pressure of nitrogen (pN_2) has no effect on the characteristics of the deposits and the deposition rate. The flow rates of each composition gas were regulated by precise needle valves and measured by a flow meter.

TABLE I Experimental conditions

Deposition temperature	450–750°C
Total gas flow rate	1–8 l min^{-1}
Gas composition:	
$pFe(C_5H_5)_2$	0–12 × 10^{-4} atm
pNH_3	0–0.9 atm
pH_2	0–0.8 atm
pCO_2	0–0.3 atm
Reaction time	120 min

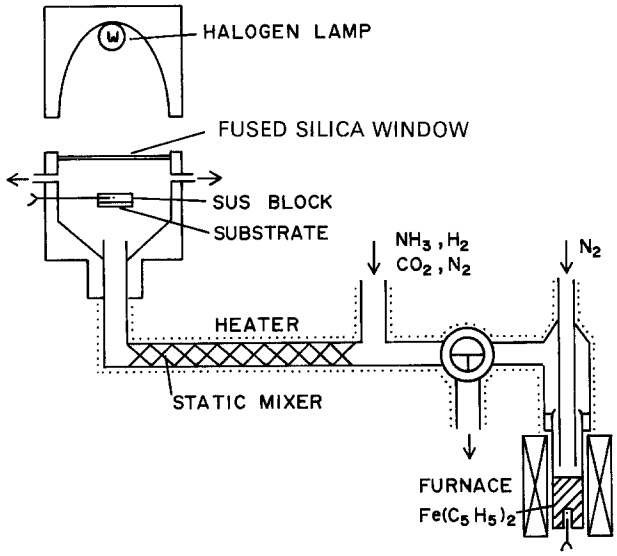

Figure 1 Schematic diagram of the apparatus.

The mixture of ferrocene vapour and other gases was faced through a nozzle (internal diameter 22 mm) to a fused silica substrate (10 mm × 10 mm × 0.5 mm) in the reactor. The distance between the top of the nozzle and the substrate was 30 mm. The diameter of the nozzle and the distance between the nozzle and the substance did not affect the uniformity and/or the deposition rate of the deposits within the range from 10 to 30 mm and 10 to 40 mm, respectively. The substrate was fixed to a stainless steel block and heated by a halogen lamp through a fused silica window at the top of the reactor. The gas line of $Fe(C_5H_5)_2$ from the vapour generator to the reactor was heated to prevent the condensation of the ferrocene vapour. The deposition conditions are summarized in Table I.

The deposition rate was determined as the weight gain of the substrate per unit area and time. The phases of the deposits and their lattice parameters were determined by X-ray diffractometry. The nitrogen and carbon contents of the deposits were determined by quantitative elemental analysis (Yanagi moto Co. Ltd, MT-2). Magnetic properties were measured using a vibrating-sample magnetometer (VSM) (Riken Densi Co. Ltd, BHV-3). σ_s was calculated per unit weight which was determined from the weight loss of the sample when the deposit was washed off the substrate using hydrochloric acid.

3. Results and discussion

3.1. Effect of deposition temperature

3.1.1. Deposition behaviour and the deposition rate

Fig. 2 shows the dependence of the deposition rate on the deposition temperature at some total gas flow rates under the fixed partial pressures of $Fe(C_5H_5)_2$ ($pFe(C_5H_5)_2$) and CO_2 (pCO_2) which were 3.0 × 10^{-4} and 0.025 atm, respectively. Two conditions were selected for the partial pressures of NH_3

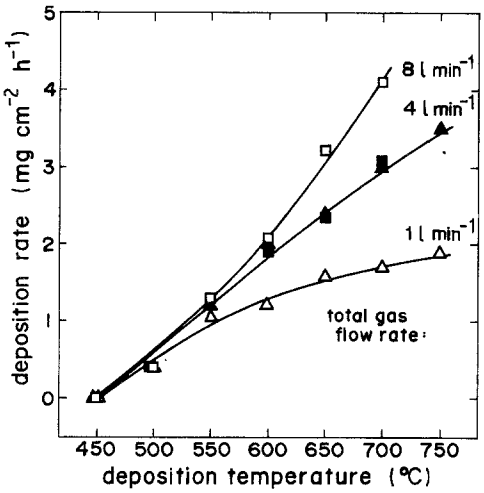

Figure 2 Dependence of the deposition rate on the deposition temperature for various total gas flow rates. $p\mathrm{Fe(C_5H_5)_2}$ = 3.0 × 10^{-4} atm, $p\mathrm{CO_2}$ = 0.025 atm. (△, ▲) $p\mathrm{NH_3}$ = 0.05 atm, $p\mathrm{H_2}$ = 0.3 atm; (□, ■) $p\mathrm{NH_3}$ = 0.1 atm, $p\mathrm{H_2}$ = 0.6 atm.

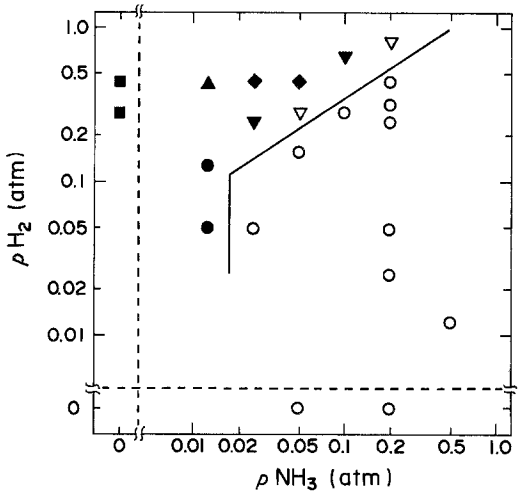

Figure 4 Dependence of the phases of the films on $p\mathrm{NH_3}$ and $p\mathrm{H_2}$ at 600° C. $p\mathrm{Fe(C_5H_5)_2}$ = 3.0 × 10^{-4} atm, $p\mathrm{CO_2}$ = 0.025 atm, total gas flow rate = 4 l min^{-1}. (■) α-Fe + C, (▲) α-Fe + Fe_3C, (◆) γ′-Fe_4N + Fe_3C, (▽) ε-Fe_2N + γ′-Fe_4N, (▼) γ′-Fe_4N + ε-Fe_2N + Fe_3C, (○) ε-Fe_2N, (●) ε-Fe_2N + Fe_3C.

($p\mathrm{NH_3}$) and H_2 ($p\mathrm{H_2}$) because of the limitation of the apparatus. Regardless of the total gas flow rate, there were very few deposits below 450° C. Deposition, however, occurred above 500° C and the deposition rate increased with increasing deposition temperature at any total gas flow rate, $p\mathrm{NH_3}$ and $p\mathrm{H_2}$.

When the deposition temperature was below 550° C, the colour of the deposits was somewhat dark-grey. Moreover, after washing off deposits with a hydrochloric acid, a black residue was observed on the substrate which showed the existence of free carbon in the deposit. On the other hand, the colour of the deposits which were obtained above 600° C was metallic grey. Thus the contents of free carbon in the deposits is lower above 600° C than below 550° C. As a result, free carbon tends to be deposited at a lower deposition temperature.

3.1.2. Composition and phases of the deposits

The dependence of nitrogen and carbon contents of the deposits on the deposition temperature is shown in Fig. 3 under the following fixed conditions: $p\mathrm{Fe(C_5H_5)_2}$ = 3.0 × 10^{-4} atm, $p\mathrm{NH_3}$ = 0.05 atm,

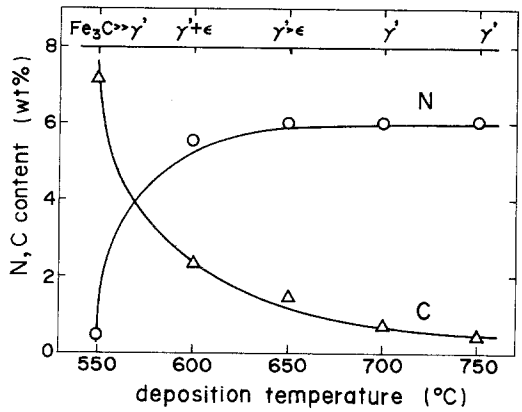

Figure 3 Dependence of nitrogen and carbon contents, and the phases of the deposits, on the deposition temperature. $p\mathrm{Fe(C_5H_5)_2}$ = 3.0 × 10^{-4} atm, $p\mathrm{NH_3}$ = 0.05 atm, $p\mathrm{H_2}$ = 0.3 atm, $p\mathrm{CO_2}$ = 0.025 atm, total gas flow rate = 4 l min^{-1}. (γ′) γ′-Fe_4N, (ε) ε-Fe_2N.

$p\mathrm{H_2}$ = 0.3 atm, $p\mathrm{CO_2}$ = 0.025 atm, total gas flow rate = 4 l min^{-1}. The phases of the deposits are also represented in Fig. 3. At 550° C the nitrogen content was small but the carbon content was large, ~7.2 wt %, which caused the major phase of the deposit to be Fe_3C. As the deposition temperature increased, the nitrogen contents increased abruptly and reached an almost constant value of about 6.0 wt % above 650° C. On the other hand, the carbon contents decreased with increasing deposition temperature and reached about 0.3 wt % at 750° C.

Thermodynamically, the phases of the deposits depended on temperature and composition. Because the films deposited in the present study consisted of iron, nitrogen and carbon, some of iron nitrides, iron carbides, iron carbonitrides or free carbon are considered to be deposited. If carbon exists only as free carbon, the atomic ratio of nitrogen to iron determines the iron nitride phase, while if the carbon atoms are dissolved in iron nitrides, the amount of iron, carbon and nitrogen atoms will decide the iron carbonitride phases. The film consisting of γ′-Fe_4N single phase involved about 0.5 to 1.0 wt % carbon atoms at 700° C as shown in Fig. 3. From the phase diagram of the Fe–N–C system [28], the solubility of carbon in γ′-Fe_4N is about 0.2 wt % at 700° C, so that the carbon in the deposits is thought to exist mainly as free carbon. However, although the nitrogen content of the film at 650° C was almost unchanged compared with that at 700° C, which was within the homogeneous range of γ′-Fe_4N, ε-Fe_2N was codeposited with γ′-Fe_4N. This showed that some carbon atoms dissolved in iron nitride phase at 650° C. On the basis of this result, the whole carbon content of the deposits could be an important factor for dissolving the carbon atoms in the iron nitride phase.

Fig. 4 shows the dependence of the phases of the deposits on $p\mathrm{NH_3}$ and $p\mathrm{H_2}$ at 600° C under the conditions of $p\mathrm{Fe(C_5H_5)_2}$ = 3.0 × 10^{-4} atm, $p\mathrm{CO_2}$ = 0.025 atm, total gas flow rate = 4 l min^{-1}. As shown in Fig. 4 the single phase of ε-Fe_2N was deposited but

the single phases of γ'-Fe_4N and α-Fe were not obtained, which was different from the results at 700° C (for details see Section 3.2.3). Instead of these, the carbide phase, Fe_3C, was codeposited with α-Fe, γ'-Fe_4N or ε-Fe_2N under a large excess pH_2 compared to pNH_3, and the carbon phase was codeposited with α-Fe in the absence of NH_3. This suggests that the carbon contents of the deposits were higher at 650° C than at 700° C, which was predicted by the results in Fig. 3. At 700° C the maximum solubilities of carbon in α-Fe, γ'-Fe_4N and ε-Fe_2N are 0.1, 0.2 and 3.0 wt %, respectively [28]. It is probably caused by the difference in the maximum solubilities of these phases that ε-Fe_2N could be deposited as single phase, while α-Fe and γ'-Fe_4N could not exist as single phase at 600° C as shown in Fig. 4. From these results, the phases deposited at 600° C may be thought to be affected by not only the nitrogen atom but also the carbon atoms in the deposits, so that these must be considered to be the phases in the Fe–C–N system. This result was in good agreement with the assumption in Fig. 3. Therefore the phases were not determined only by $pNH_3/pH_2^{3/2}$, which assigned the nitrogen content in the deposits at 700° C. As a result, the phase boundary line between different phases in Fig. 4 was unclear compared with that at 700° C, as shown in Fig. 8 (for details see Section 3.2.3).

3.2. Effect of gas composition and total gas flow rate at 700° C

3.2.1. Deposition behaviour

The effect of pNH_3 and pH_2 on the deposition behaviour was studied at 700° C. The experimental conditions were $pFe(C_5H_5)_2 = 3.0 \times 10^{-4}$ atm, $pCO_2 = 0.025$ atm, total gas flow rate = 4 l min^{-1}. The effects of pNH_3 and pH_2 were roughly divided into three regions from the difference in the deposition behaviour. In the absence both of NH_3 and H_2, there was little deposit on the substrate. On the other hand, in the absence of NH_3 or large excess of H_2 compared with NH_3, a deposit was obtained but it consisted of fine particles. However, in the third case, a dense film was obtained. In brief, hydrogen is essential for the preparation of the deposits and a certain pNH_3 is needed for the preparation of the films. Because the deposits are formed through the decomposition of $Fe(C_5H_5)_2$ (for details see Section 3.2.2), NH_3 must accelerate the decomposition of $Fe(C_5H_5)_2$. In subsequent sections we are mainly concerned with the region where the dense film is obtained.

3.2.2. Deposition rate

Fig. 5 represents the relationship between the reaction time and the deposition weight per unit area for various pNH_3, pH_2 and $pFe(C_5H_5)_2$ under a fixed total gas flow rate of 4 l min^{-1} and pCO_2 of 0.025 atm. The deposition weight increased linearly with increasing reaction time irrespective of the gas composition up to 120 min. Moreover, it was also ascertained that the phases and the microstructures of the films did not change remarkably depending on the reaction time. Therefore, the deposition mechanism which is estimated from the deposition rate, may be unaffected by the reaction time.

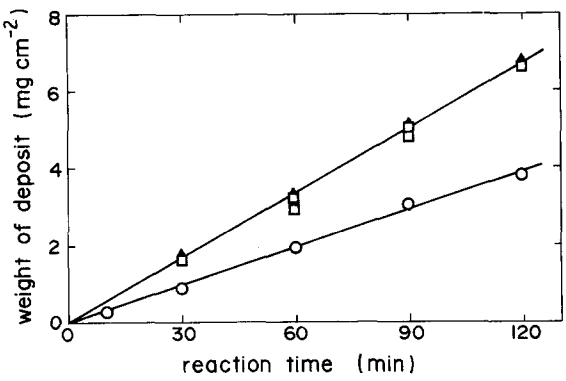

Figure 5 Weight of deposit plotted against reaction time at 700° C for various $pFe(C_5H_5)_2$, pNH_3, pH_2. $pCO_2 = 0.025$ atm, total gas flow rate = 4 l min^{-1}. (□) $pFe(C_5H_5)_2 = 3.0 \times 10^{-4}$ atm, $pNH_3 = 0.05$ atm, $pH_2 = 0.3$ atm; (○) $pFe(C_5H_5)_2 = 1.8 \times 10^{-4}$ atm, $pNH_3 = 0.05$ atm, $pH_2 = 0.3$ atm; (▲) $pFe(C_5H_5)_2 = 3.0 \times 10^{-4}$ atm, $pNH_3 = 0.2$ atm, $pH_2 = 0.75$ atm.

Fig. 6 shows the dependence of the deposition rate on $pFe(C_5H_5)_2$ at some total gas flow rate under a fixed pCO_2 of 0.025 atm. Two conditions were selected for pNH_3 and pH_2 because of the limitations of the apparatus. However, it has been already confirmed that deposition rate was independent of pNH_3 and pH_2 under a total gas flow rate from 1 to 8 l min^{-1}, which was shown, for example, in Figs 2 and 5 under 4 l min^{-1}. As shown in Fig. 6, the deposition rate increased linearly with $pFe(C_5H_5)_2$ irrespective of the total gas flow rate. Moreover, the deposition rate increased with increasing total gas flow rate under fixed $pFe(C_5H_5)_2$.

Fig. 7 shows the data in Fig. 6 plotted as log deposition rate against log total gas flow rate under a fixed $pFe(C_5H_5)_2$ of 4.0×10^{-4} atm. The linear relationship in Fig. 7 suggests that the deposition rate is controlled by the mass transport in the gas phase under a total gas flow rate from 1 to 8 l min^{-1}. The slope of the line in Fig. 7 is about 0.48 which is almost equivalent to the theoretical one, 0.5 [29]. On the other hand, as shown in Fig. 7, the deposition rate of each film depends not on pNH_3, pH_2 and pCO_2 but only

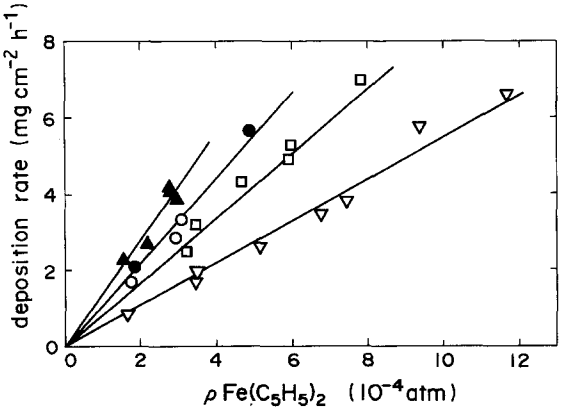

Figure 6 Deposition rate plotted against $pFe(C_5H_5)_2$ for various total gas flow rates at 700° C and under pCO_2 of 0.025 atm. (▲) 8 l min^{-1}, (●, ○) 4 l min^{-1}, (□) 2 l min^{-1}, (▽) 1 l min^{-1}. (▲, ●) $pNH_3 = 0.1$ atm, $pH_2 = 0.6$ atm; (○, □, ▽) $pNH_3 = 0.05$ atm, $pH_2 = 0.3$ atm.

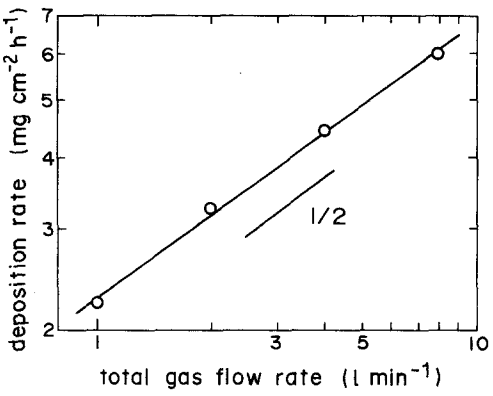

Figure 7 Log deposition rate plotted against total gas flow rate at the deposition temperature of 700° C. $p\mathrm{Fe}(\mathrm{C_5H_5})_2 = 4.0 \times 10^{-4}$ atm, $p\mathrm{CO_2} = 0.025$ atm.

linearly on $p\mathrm{Fe}(\mathrm{C_5H_5})_2$. Therefore, the transport of $\mathrm{Fe}(\mathrm{C_5H_5})_2$ molecules to the surface of the deposits may be the rate-determining step at 700° C and under the total gas flow rate from 1 to 8 l min^{-1}. Hence under these conditions, the $\mathrm{Fe}(\mathrm{C_5H_5})_2$ molecule arrives at the surface of the substrate and decomposes immediately to produce deposits.

3.2.3. Phases of the deposit

3.2.3.1. Effect of pNH_3 and pH_2. Fig. 8 shows the effect of $p\mathrm{NH_3}$ and $p\mathrm{H_2}$ on the phases of the films at 700° C and under a total gas flow rate of 4 l min^{-1}. Other experimental conditions were the same as shown in Fig. 4 at 600° C. As already reported [24], the films consisting of the single phases of α-Fe, γ′-$\mathrm{Fe_4N}$ and ε-$\mathrm{Fe_2N}$ and the mixed phases of α-Fe + γ′-$\mathrm{Fe_4N}$ and γ′-$\mathrm{Fe_4N}$ + ε-$\mathrm{Fe_2N}$ were deposited depending on $p\mathrm{NH_3}$ and $p\mathrm{H_2}$. Peaks related to ζ-$\mathrm{Fe_2N}$ were observed accompanying ε-$\mathrm{Fe_2N}$ on the X-ray diffraction (XRD) pattern of the films, which contain excess nitrogen in ε-$\mathrm{Fe_2N}$. However, ε-$\mathrm{Fe_2N}$ and ζ-$\mathrm{Fe_2N}$ could not be quantitatively divided using XRD, so that we describe them together as "ε-$\mathrm{Fe_2N}$" in this paper.

In Fig. 8 the boundary lines between different phase

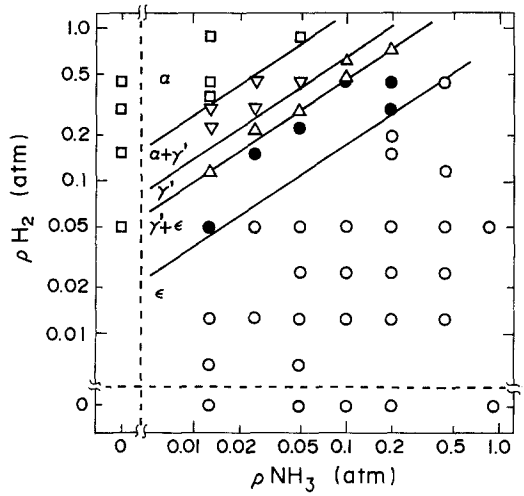

Figure 8 Effects of $p\mathrm{NH_3}$ and $p\mathrm{H_2}$ on the phases of the films at 700° C. $p\mathrm{Fe}(\mathrm{C_5H_5})_2 = 3.0 \times 10^{-4}$ atm, $p\mathrm{CO_2} = 0.025$ atm, total gas flow rate = 4 l min^{-1}. (□) α-Fe, (▽) α-Fe + γ′-$\mathrm{Fe_4N}$, (△) γ′-$\mathrm{Fe_4N}$, (●) γ′-$\mathrm{Fe_4N}$ + ε-$\mathrm{Fe_2N}$, (○) ε-$\mathrm{Fe_2N}$.

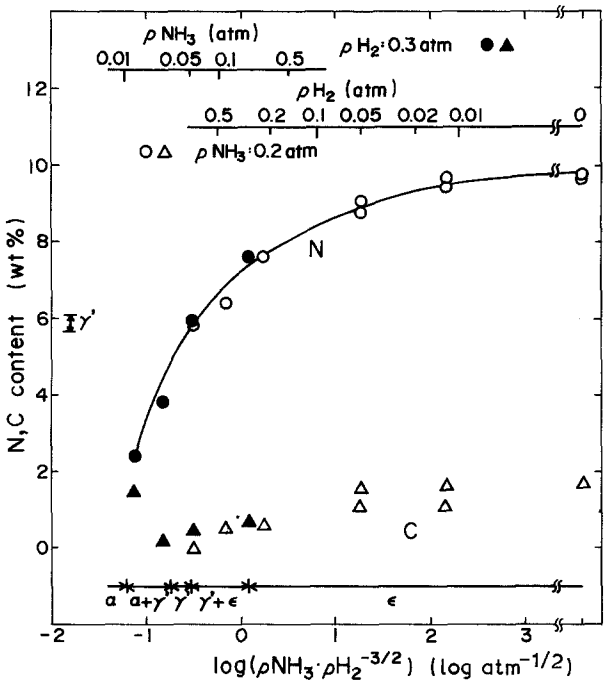

Figure 9 Nitrogen and carbon contents and phases of the films as a function of $p\mathrm{NH_3}/p\mathrm{H_2}^{3/2}$ at 700° C. $p\mathrm{Fe}(\mathrm{C_5H_5})_2 = 3.0 \times 10^{-4}$ atm, $p\mathrm{CO_2} = 0.025$ atm, total gas flow rate = 4 l min^{-1}. (α) α-Fe, (γ′) γ′-$\mathrm{Fe_4N}$, (ε) ε-$\mathrm{Fe_2N}$, (●, ▲) $p\mathrm{H_2} = 0.3$ atm, (○, △) $p\mathrm{NH_3} = 0.2$ atm.

regions are represented by

$$p\mathrm{NH_3}/p\mathrm{H_2}^{3/2} = K \qquad (2)$$

where K is constant. Equation 2 is known as the nitriding potential of the $\mathrm{NH_3}$–$\mathrm{H_2}$ mixture [30]. As $p\mathrm{NH_3}/p\mathrm{H_2}^{3/2}$ increased, the phases with higher nitrogen content tended to be deposited, such as α-Fe → α-Fe + γ′-$\mathrm{Fe_4N}$ → γ′-$\mathrm{Fe_4N}$ → γ′-$\mathrm{Fe_4N}$ + ε-$\mathrm{Fe_2N}$ → ε-$\mathrm{Fe_2N}$. The values of $p\mathrm{NH_3}/p\mathrm{H_2}^{3/2}$ corresponding to each phase region are summarized in Table II.

Fig. 9 shows the nitrogen and carbon contents and the phases of the films as a function of $p\mathrm{NH_3}/p\mathrm{H_2}^{3/2}$ for constant $p\mathrm{NH_3}$ (0.2 atm) and $p\mathrm{H_2}$ (0.3 atm) under the conditions in Fig. 8. Under fixed $p\mathrm{NH_3}$ and $p\mathrm{H_2}$, the change in $p\mathrm{NH_3}/p\mathrm{H_2}^{3/2}$ corresponds to that of $p\mathrm{H_2}$ and $p\mathrm{NH_3}$, respectively, which is also represented in Fig. 9. The nitrogen contents of the deposits increased with increasing $p\mathrm{NH_3}/p\mathrm{H_2}^{3/2}$. This increase makes the phase change from a nitrogen-poor phase to a nitrogen-rich one in good agreement with the phase diagram of the Fe–N system [1]. Fig. 9 shows that the nitrogen contents and the phases of the films were regulated by $p\mathrm{NH_3}/p\mathrm{H_2}^{3/2}$ under any ratio of $p\mathrm{NH_3}$ and $p\mathrm{H_2}$ where $p\mathrm{Fe}(\mathrm{C_5H_5})_2$ and temperature were constant. On the other hand, the dependence of the carbon contents on

TABLE II Range of $p\mathrm{NH_3}/p\mathrm{H_2}^{3/2}$ over which the various iron nitride phases are deposited at 700° C. $p\mathrm{Fe}(\mathrm{C_5H_5})_2 = 3.0 \times 10^{-4}$ atm, $p\mathrm{CO_2} = 0.025$ atm, total gas flow rate = 4 l min^{-1}

Phases	$p\mathrm{NH_3}/p\mathrm{H_2}^{3/2}$ (atm$^{-1/2}$)
α-Fe	⩽0.06
α-Fe + γ′-$\mathrm{Fe_4N}$	0.06–0.18
γ′-$\mathrm{Fe_4N}$	0.18–0.30
γ′-$\mathrm{Fe_4N}$ + ε-$\mathrm{Fe_2N}$	0.30–1.2
ε-$\mathrm{Fe_2N}$	⩾1.2

$pNH_3/pH_2^{3/2}$ could not be elucidated within the experimental limits of the present study, as shown in Fig. 9.

From the present results we can consider the mechanism of NH_3 decomposition under the conditions in Fig. 8; NH_3 molecules adsorb and dissociate on the surface of the substrate as follows

$$2NH_3(ad) \rightarrow 2N(ad) + 3H_2 \quad (3)$$

$$2N(ad) \rightarrow N(\text{in Fe–N}) \quad (4)$$

where (ad) and N(in Fe–N) mean chemical species adsorbed on the surface and nitrogen dissolving in the iron nitride phase, respectively. Moreover Reaction 4, dissolving in the iron nitride phase, is the rate-determining step, and the decomposition rate of NH_3, r, can be represented by

$$r = k(pNH_3^2/pH_2^3)^{1-\alpha} \quad (5)$$

where α is a semiempirical constant obtained by assuming the heat of NH_3 adsorption to be a linear function of NH_3 coverage on the surface. Therefore, $pNH_3/pH_2^{3/2}$ determines the amount of nitrogen on the surface, i.e. the determining factor of nitrogen activity. This mechanism is called the Temkin–Pyzhev mechanism [31]. Moreover, as described in Section 3.2.2., $Fe(C_5H_5)_2$ molecules arriving at the surface of the deposits decompose immediately to produce films, because the rate-determining step of the deposition may be the transport of $Fe(C_5H_5)_2$ molecules. Therefore, under constant $pFe(C_5H_5)_2$, $pNH_3/pH_2^{3/2}$ determines the ratio of iron to nitrogen on the surface, which also determines the phase of the deposits. As a result, the boundary lines between different phase regions, are represented by Equation 2 as shown in Fig. 8.

3.2.3.2. Effect of $pFe(C_5H_5)_2$. Fig. 10 shows the effects of $pFe(C_5H_5)_2$ and total gas flow rate on the phases of the films under pCO_2 of 0.025 atm at 700° C. The ratios of pNH_3 and pH_2, i.e. $pNH_3/pH_2^{3/2}$, were selected in the region where the single phase of γ'-Fe_4N was deposited when $pFe(C_5H_5)_2$ was 3.0×10^{-4} atm as shown in Fig. 8. As $pFe(C_5H_5)_2$ increased, the kind of the phases in the films changed from single-phase of γ'-Fe_4N to mixed phase γ'-Fe_4N and ε-Fe_2N above 2 l min^{-1}. This phase change cannot be explained only by the effect of the nitrogen contents of the films. Under constant pNH_3 and pH_2, the increase in $pFe(C_5H_5)_2$ causes an increase in the atomic ratio of iron to nitrogen on the surface of the substrate, so that the phase with lower nitrogen, perhaps α-Fe, should be codeposited with γ'-Fe_4N. This phase change can be explained by the effect of the carbon contents of the films on the phases as follows: as $pFe(C_5H_5)_2$ increases, the carbon contents of the films will increase accompanied by increasing iron contents. Therefore the solubility of carbon atoms in the nitride phase becomes large, and ε-Fe_2N is thought to be codeposited with γ'-Fe_4N. On the other hand, Fe_3C instead of ε-Fe_2N was codeposited with increasing $pFe(C_5H_5)_2$ under a total gas flow rate of 1 l min^{-1}. This phase change could not be explained solely by increasing carbon content at the surface of the deposits, so that the desorption of carbon atom from the surface of the deposits must also be considered.

3.2.3.3. Effect of pCO_2. The nitrogen and carbon contents of the films as a function of pCO_2 at 700° C are shown in Fig. 11. The experimental conditions are $pNH_3 = 0.0125$ atm, $pH_2 = 0.3$ atm, $pFe(C_5H_5)_2 = 3.0 \times 10^{-4}$ atm, total gas flow rate = 4 l min^{-1}. As shown in Fig. 8, this condition corresponds to the region where γ'-Fe_4N is codeposited with α-Fe under pCO_2 of 0.025 atm. The phases of the deposits are also represented in Fig. 11.

When CO_2 is not introduced into the reactor, the nitrogen content is small but the carbon content is large, ~4.5 wt % so that Fe_3C is codeposited with α-Fe and γ'-Fe_4N as shown in Fig. 11. As pCO_2 increased, the nitrogen contents of the deposits increased gradually but the carbon contents decreased abruptly and reached a constant at about 1.6 wt % above 0.025 atm pCO_2. In addition, the fraction of γ'-Fe_4N was increased compared with that of α-Fe. It is possible to give an explanation for this phenomenon as follows: if excess CO_2 is introduced into the system, the following reaction will occur together with Reaction 1

$$CO_2 + H_2 \rightarrow CO + H_2O \quad (6)$$

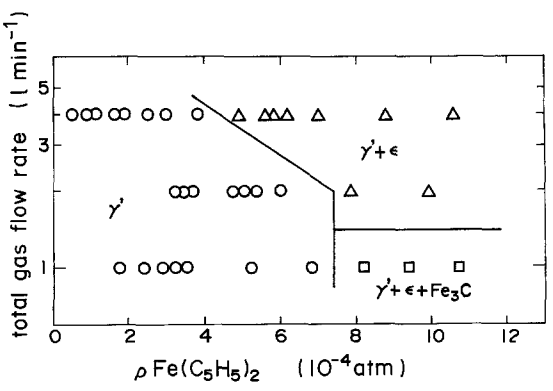

Figure 10 Effects of $pFe(C_5H_5)_2$ and total gas flow rate on the phases of the films deposited at 700° C for various pNH_3, pH_2. $pFe(C_5H_5)_2 = 3.0 \times 10^{-4}$ atm, $pCO_2 = 0.025$ atm, (○) γ'-Fe_4N, (△) γ'-Fe_4N + ε-Fe_2N, (□) γ'-Fe_4N + ε-Fe_2N + Fe_3C.

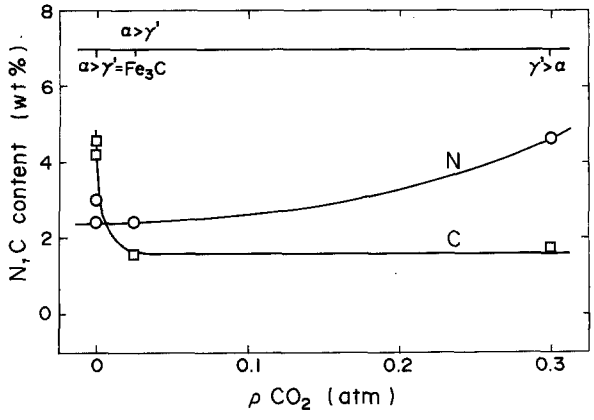

Figure 11 Nitrogen and carbon contents and the phases of the films as a function of pCO_2. Deposition temperature = 700° C. $pFe(C_5H_5)_2 = 3.0 \times 10^{-4}$ atm, $pNH_3 = 0.0125$ atm, $pH_2 = 0.3$ atm, total gas flow rate = 4 l min^{-1}. (α) α-Fe, (γ') γ'-Fe_4N.

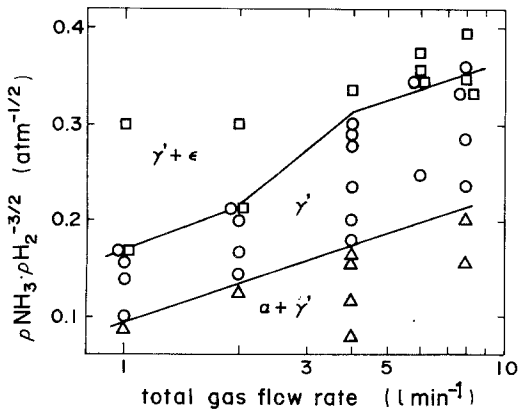

Figure 12 Effects of $pNH_3/pH_2^{3/2}$ and total gas flow rate on the phases of the films deposited at 700° C. $pFe(C_5H_5)_2 = 3.0 \times 10^{-4}$ atm, $pCO_2 = 0.025$ atm. (□) γ'-Fe_4N + ε-Fe_2N, (○) γ'-Fe_4N, (△) α-Fe + γ'-Fe_4N.

Reaction 6 reduces pH_2, so that $pNH_3/pH_2^{3/2}$, i.e. the nitrogen content of the deposits, increases as shown in Fig. 11. On the basis of the results shown in Fig. 11, it can be considered that the reduction in carbon contents of the films by introducing CO_2 into the reactor has been successfully achieved. In general, removal of carbon from the films by CO_2 seems to be more effective when the value of $pNH_3/pH_2^{3/2}$ is small.

3.2.3.4. Effect of total gas flow rate. Fig. 12 shows the effects of $pNH_3/pH_2^{3/2}$ and total gas flow rate on the phases of the deposits at 700° C and under fixed $pFe(C_5H_5)_2$ of 3.0×10^{-4} atm and pCO_2 of 0.025 atm. As shown in Fig. 12, under the fixed $pNH_3/pH_2^{3/2}$, the phase with lower nitrogen content was deposited with increasing total gas flow rate. This means that under the fixed $pNH_3/pH_2^{3/2}$, the nitrogen content of the films, which is decided by $pNH_3/pH_2^{3/2}$, decreases with increasing total gas flow rate.

On the other hand, with increasing total gas flow rate the deposition rate, which was determined by the deposition weight per unit time and area, increased under the fixed $pFe(C_5H_5)_2$ as shown in Fig. 6. Because most of the weight deposited depended on the weight of iron atoms, the deposition of iron also increased. The phases of the films were determined by the ratio of iron to nitrogen on the surface, so that the nitrogen on the surface must be decreased with increasing total gas flow rate. This result was in good agreement with the results of Fig. 12.

3.3. Characteristics of the deposits

3.3.1. Lattice parameters of ε-Fe_2N deposited at 700° C

As mentioned in Section 3.1.2, films obtained in the present study consisted of iron, nitrogen and carbon. When carbon atoms are dissolved in ε-Fe_2N, the lattice parameters of ε-Fe_2N are known to change according to total number of interstitial atoms (N + C) and their ratio (N/C) [32, 33]. In the present study, the effect of (N/C) seems to be negligible compared with that of (N + C), because the effect of (N + C) on the lattice parameters of ε-Fe_2N is generally larger than that of (N/C) [32, 33] and the maximum value of (N/C) is less than 25% as shown in

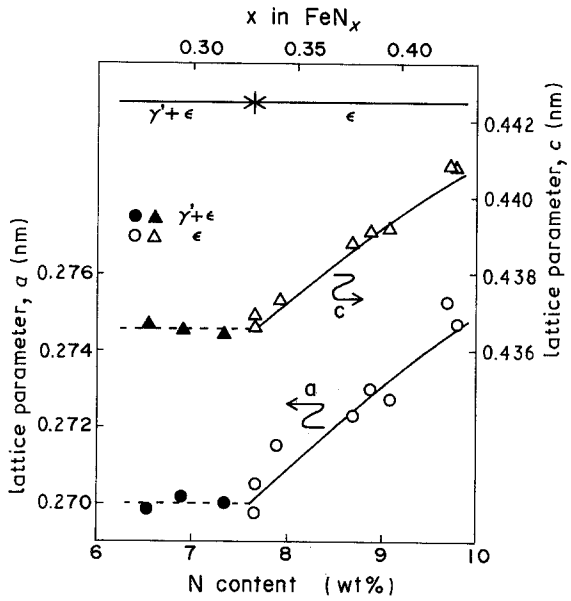

Figure 13 Dependence of lattice parameters of ε-Fe_2N and the phases of the films on the nitrogen content of the films deposited at 700° C. $pFe(C_5H_5)_2 = 3.0 \times 10^{-4}$ atm, $pCO_2 = 0.025$ atm, total gas flow rate = 4 l min^{-1}, (○, △) ε-Fe_2N, (●, ▲) ε-Fe_2N + γ'-Fe_4N.

Fig. 8 even if no free-carbon is present in the films. Therefore, it can be considered that the lattice parameters of ε-Fe_2N are mainly affected by (N + C).

The dependence of lattice parameters of ε-Fe_2N deposited at 700° C on the nitrogen contents of the films is shown in Fig. 13, together with the phases of the films deposited. Other deposition conditions were $pFe(C_5H_5)_2 = 3.0 \times 10^{-4}$ atm, $pCO_2 = 0.025$ atm, total gas flow rate = 4 l min^{-1}. Although the films were deposited under different conditions of pNH_3 and pH_2, the lattice parameters of ε-Fe_2N depended not on the deposition conditions but on the nitrogen content of the films. As shown in Fig. 13, the lattice parameter change could be divided into two regions by the kind of deposit in the phase: the region of ε-Fe_2N single phase and the mixed phases of ε-Fe_2N + γ'-Fe_4N. In the former region, the lattice parameters increased with increasing nitrogen content of the films. This result agrees well with previous data given by Jack [34] in the Fe–N system shown by the solid lines in Fig. 13. Jack obtained this result for α-Fe powder nitrided in a gaseous mixture of NH_3 and H_2. This suggests that the lattice parameter change of ε-Fe_2N can be explained only by the nitrogen content of the deposits, which is related to the nitrogen atom in the ε-Fe_2N structure.

On the other hand, the lattice parameters of ε-Fe_2N were almost constant where γ'-Fe_4N coexisted with ε-Fe_2N. The nitrogen content of ε-Fe_2N can be estimated from this constant lattice parameter using Jack's data to be about 7.8 wt %, which agrees with the nitrogen deficient limit of ε-Fe_2N shown in Fig. 13. Considering that the homogeneous range of γ'-Fe_4N is limited, the change in the nitrogen content of the films in this region mainly corresponds to the fraction change of ε-Fe_2N to γ'-Fe_4N, where the nitrogen contents are 7.8 and 5.7 to 6.1 wt %, respectively.

In brief, this means that at 700° C the effect of carbon atoms on the lattice parameters of ε-Fe_2N is

negligible, and confirms that carbon atoms in the film seem to exist mainly as free carbon, as described in Section 3.1.2.

3.3.2. Microstructure and magnetic properties

3.3.2.1. Saturation magnetization. The dependence of σ_s on the nitrogen contents of the films is shown in Fig. 14. The deposition conditions of the film were deposition temperature = 700° C, $p\mathrm{Fe}(C_5H_5)_2$ = 3.0×10^{-4} atm, $p\mathrm{CO}_2$ = 0.025 atm, total gas flow rate = 4 l min^{-1}. Although the films were deposited under different conditions for $p\mathrm{NH}_3$ and $p\mathrm{H}_2$, σ_s also depends not on the conditions of $p\mathrm{NH}_3$ and $p\mathrm{H}_3$ but on the nitrogen contents of the films. σ_s decreased with increasing nitrogen content, as shown in Fig. 14. In particular, the linear relationship holds above 5.7 wt % nitrogen content. This tendency is compatible with that reported for the bulk iron nitride materials [35–37]. In addition, σ_s of the films consisting of γ'-Fe_4N single phase was 188 e.m.u. g^{-1}, which was almost equivalent to the reported value for the bulk material, 192 e.m.u. g^{-1}. This suggests that the effects of oxidation on introducing CO_2 into the system and/or the carbon contamination in the films are negligibly small.

3.3.2.2. Coercive force and microstructure as a parameter of deposition temperature. The dependence of coercive force of the deposits, H_c, on the deposition temperature is shown in Fig. 15. Deposition conditions were $p\mathrm{Fe}(C_5H_5)_2$ = 3.0×10^{-4} atm, $p\mathrm{NH}_3$ = 0.05 atm, $p\mathrm{H}_2$ = 0.3 atm, $p\mathrm{CO}_2$ = 0.025 atm, total gas flow rate = 4 l min^{-1}. Deposition conditions were the same as those in Fig. 3. Although H_c was almost constant at 30 Oe above 600° C, the films deposited at 550° C had an extremely high H_c. This rapid change in H_c seemed to be caused by the change in microstructure of the films.

Fig. 16 shows typical microstructures of the surface and fractured surface of the films deposited at (ab) 550° C, and (c,d) 700° C which corresponds to the typical microstructure above 600° C. At 700° C the microstructure of the film was dense, uniform and made up of angular grains with stripes on their surface, as shown in Fig. 16c, d. At 550° C, the characteristics of the microstructure were small plate-like particles and interstices between particles as shown in Fig. 16a, b. These interstices and the magnetic anisotropy of each plate-like particle seem to cause the high H_c of the films.

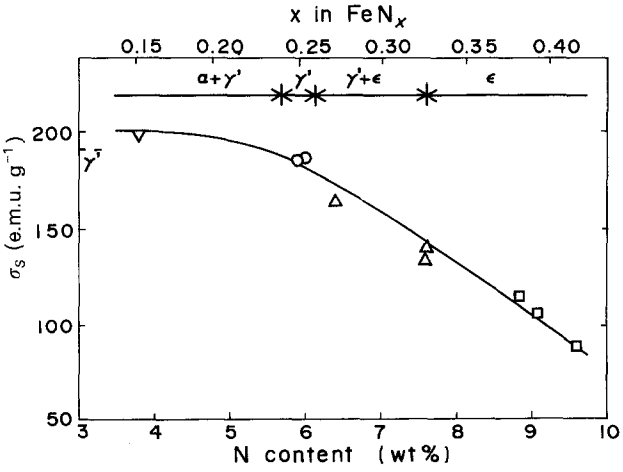

Figure 14 σ_s plotted against nitrogen content of the films deposited for various conditions of $p\mathrm{NH}_3$ and $p\mathrm{H}_2$. Deposition temperature = 700° C, $p\mathrm{Fe}(C_5H_5)_2$ = 3.0×10^{-4} atm, $p\mathrm{CO}_2$ = 0.025 atm, total gas flow rate = 4 l min^{-1}. (▽) α-Fe + γ'-Fe_4N, (○) γ'-Fe_4N, (△) γ'-Fe_4N + ε-Fe_2N, (□) ε-Fe_2N.

4. Conclusions

Iron nitride films were prepared on fused silica substrates by CVD from the gaseous mixture of $\mathrm{Fe}(C_5H_5)_2$–NH_3–H_2–CO_2 under atmospheric pressure. The effects of deposition parameters (i.e. deposition temperature, total gas flow rate and input gas composition) on the deposition characteristics, such as the deposition rate, and the phase, the microstructure, the nitrogen and carbon contents, and the magnetic properties of the deposits, were investigated. The following results were obtained.

1. Iron nitride films were deposited above 500° C and films of γ'-Fe_4N single phase were deposited above 700° C.

2. At 700° C and at a total gas flow rate of 1 to 81 min^{-1}, the transport of $\mathrm{Fe}(C_5H_5)_2$ molecules to the surface of the deposits may be the rate determining step.

3. At 700° C and at a total gas flow rate of 4 l min^{-1}, films consisting of α-Fe, γ'-Fe_4N and ε-Fe_2N were deposited and these phases were determined by $p\mathrm{NH}_3/p\mathrm{H}_2^{3/2}$ which was the factor controlling the nitrogen content of the films.

4. At a deposition temperature of 700° C, the nitrogen content of the films increased as the total gas flow rate decreased or $p\mathrm{CO}_2$ increased, so that the phase with a higher nitrogen content was codeposited. The carbon content increased with increasing $p\mathrm{Fe}(C_5H_5)_2$ or the absence of CO_2, so that the phase with greater solubility in carbon, i.e. ε-Fe_2N, was codeposited with γ'-Fe_4N.

5. The change in ε-Fe_2N lattice parameters deposited at 700° C was interpreted in terms of the nitrogen content of the films, and did not depend on the deposition conditions.

6. The change in saturation magnetization, σ_s, of the films deposited at 700° C was in good agreement with that reported for the bulk iron nitride materials, which depends not on the deposition conditions but on the nitrogen content of the films.

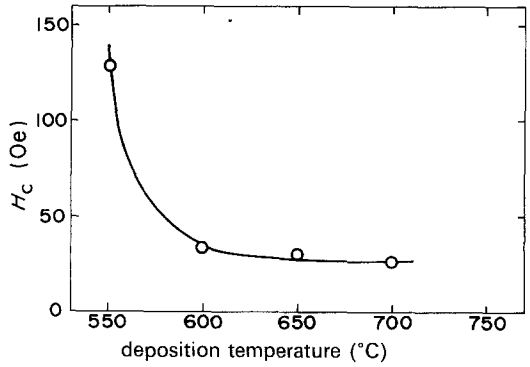

Figure 15 Dependence of coercive force of the deposits on the deposition temperature. $p\mathrm{Fe}(C_5H_5)_2$ = 3.0×10^{-4} atm, $p\mathrm{NH}_3$ = 0.05 atm, $p\mathrm{H}_2$ = 0.3 atm, $p\mathrm{CO}_2$ = 0.025 atm, total gas flow rate = 4 l min^{-1}.

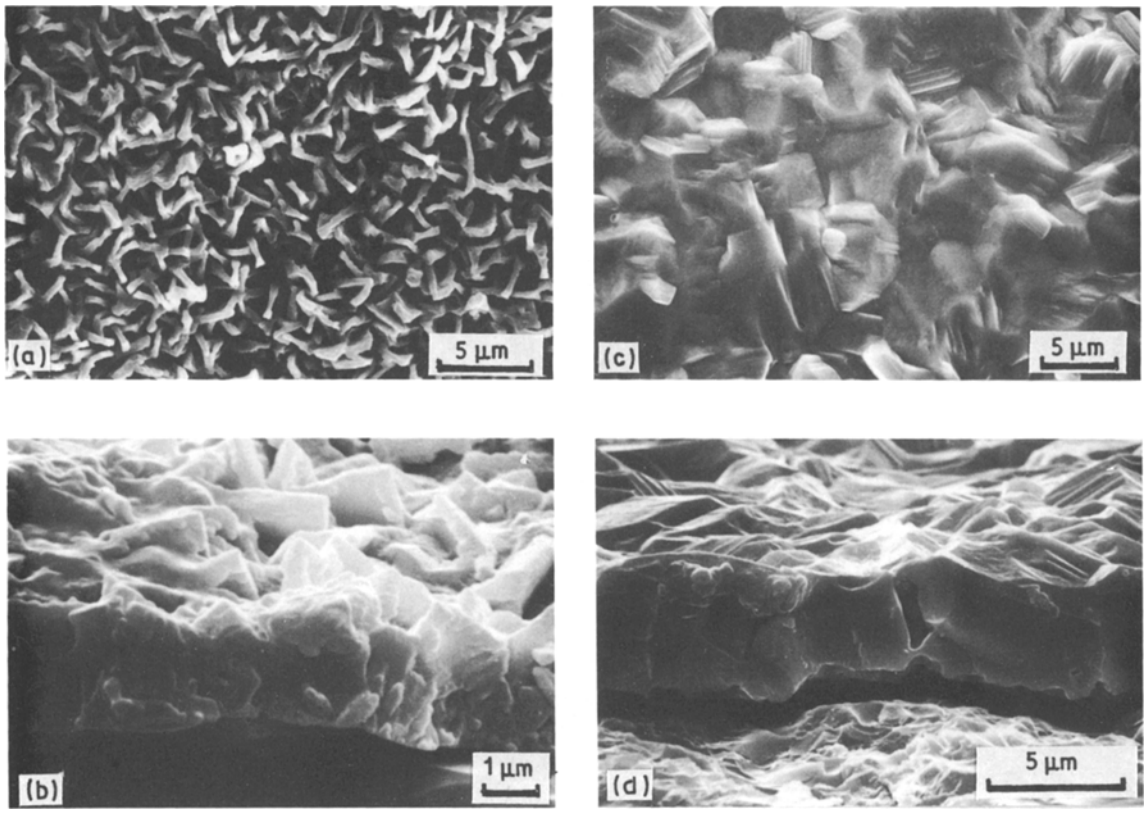

Figure 16 Scanning electron micrographs of surface and fractured surface of iron nitride films deposited at (a, b) 550° C and (c, d) 700° C. $p\mathrm{Fe}(\mathrm{C_5H_5})_2 = 3.0 \times 10^{-4}$ atm, $p\mathrm{NH_3} = 0.05$ atm, $p\mathrm{H_2} = 0.3$ atm, $p\mathrm{CO_2} = 0.025$ atm, total gas flow rate = 4 l min^{-1}.

7. The coercive force of the films deposited at 550° C was large compared with that above 550° C, which was related to the change in microstructure.

Acknowledgements

This research was supported in part by the Grant-in-Aid for Encouragement of Young Scientists from the Ministry of Education, Science and Culture under Contract no. 6 375 032. The authors thank Mr Douba, Riken Densi Co. Ltd, for measurement of the magnetic properties.

References

1. H. J. GOLDSCHMIDT, in "Interstitial Alloys" (Butterworths, London, 1967) p. 228.
2. T. K. KIM and M. TAKAHASHI, *Appl. Phys. Lett.* **20** (1972) 492.
3. K. YAMAUCHI, S. YATSUYA and K. MIHAMA, *J. Cryst. Growth* **46** (1979) 615.
4. N. SAEGUSA, T. TSUKAGOSHI, E. KITA and A. TASAKI, *IEEE Trans. Mag.* **MAG-19** (1983) 1629.
5. T. TANAKA, K. TAGAWA and A. TASAKI, *Nippon Kagaku Kaishi* (1984) 930.
6. S. SUZUKI, H. SAKUMOTO, S. MINEGISHI and Y. OMOTO, *IEEE Trans. Mag.* **MAG-17** (1981) 3017.
7. S. SUZUKI, H. SAKUMOTO, Y. OMOTE and J. MINEGISHI, *ibid.* **MAG-20** (1984) 48.
8. K. TAGAWA, E. KITA and A. TASAKI, *Jpn J. Appl. Phys.* **21** (1982) 1596.
9. V. S. ZHIGALOV, L. I. VERSHININA and G. I. FROLOV, *Sov. Phys. Solid State* **26** (1984) 1145.
10. A. KANO, N. S. KAZAMA, H. FUJIMORI and T. TAKAHASHI, *J. Appl. Phys.* **53** (1982) 8332.
11. S. ASADA and M. KITADA, *Appl. Phys. Lett.* **46** (1985) 792.
12. C. LO, S. V. KRISHNASWAMY, K. R. P. M. RAO, R. MESSIER and L. N. MULAY, *Mater. Res. Bull.* **15** (1980) 1267.
13. N. HEIMAN and N. S. KAZAMA, *J. Appl. Phys.* **52** (1981) 3562.
14. C. LO, S. V. KRISHNASWAMY, L. N. MULAY and R. A. DIFFENBACH, *ibid.* **53** (1982) 2745.
15. M. KAWARADA, N. KOSHINO and S. OGAWA, *IEEE Trans. Mag.* **MAG-23** (1987) 2973.
16. K. UMEDA, Y. KAWASHIMO, N. NAKASONE, S. HARADA and A. TASAKKI, *Jpn J. Appl. Phys.* **23** (1984) 1576.
17. N. TERADA, Y. HOSHI, M. NAOE and S. YAMANAKA, *IEEE Trans. Mag.* **MAG-20** (1986) 1451.
18. N. TERADA, M. NAOE and Y. HOSHI, *Adv. Ceram.* **16** (1985) 281.
19. K. UMEDA, E. KITA and A. TASAKI, *IEEE Trans. Mag.* **MAG-22** (1986) 591.
20. P. CHATTERJEE and A. K. BATABYAL, *Thin Solid Films* **169** (1989) 79.
21. K. NAKAJIMA, S. OKAMOTO, K. KOBAYASHI and M. IWAKI, *Nippon Kagaku Kaishi* (1987) 2001.
22. B. RAUSCHENBACH and V. HEERA, *J. Less-Common Metals* **117** (1986) 323.
23. Y. SAITO, H. TANAKA and K. FUJIMORI, *J. Mater. Sci. Lett.* **5** (1986) 1166.
24. H. FUNAKUBO, N. KIEDA, N. MIZUTANI and M. KATO, *ibid.* **7** (1988) 851.
25. G. WILKINSON and F. A. COTTON, *Prog. Inorg. Chem.* **1** (1959) 1.
26. J. T. S. ANDREWS and E. F. WESTRUM Jr, *J. Organometal. Chem.* **17** (1969) 349.
27. S. PIGNATARO and F. P. LOSSING, *ibid.* **11** (1968) 571.
28. V. RAGHAVAN, *Trans. Indian Inst. Met.* **37** (1984) 293.
29. H. SCHLICHTING, in "Boundary Layer Theory", 7th Edn (McGraw-Hill, New York, 1979).
30. D. ATKINSON and C. BODSWORTH, *J. Iron Steel Inst.* **208** (1970) 587.
31. M. I. TEMKIN and V. PYZHEV, *Acta Physiochem. USSR* **12** (1940) 327.
32. K. H. JACK, *Proc. Roy. Soc.* **A195** (1948) 41.
33. F. K. NAUMAN and G. LANGENSCHEILD, *Arch. Eisenhuttenew.* **36** (1965) 677.

34. K. H. JACK, *Acta Crystallogr.* **5** (1952) 404.
35. G. M. CHEN, N. K. JAGGL, J. B. BUTT, E. B. YEH and L. H. SCHWARTZ, *J. Phys. Chem.* **87** (1983) 5326.
36. J. B. GOODENOUGH, A. WOLD and R. J. ARNOTT, *J. Appl. Phys.* **31** (1960) 342S.
37. M. MEKATA, H. YOSHIMURA and H. TASAKI, *J. Phys. Soc. Jpn* **33** (1972) 62.

Received 8 June
and accepted 23 October 1989